Received: 15 October 2020 | Revised: 17 November 2020 | Accepted: 18 November 2020

DOI: 10.1002/pls2.10023

RESEARCH ARTICLE

SPE POLYMERS WILEY

Gas separation through polyurethane–ZnO mixed matrix membranes and mathematical modeling of the interfacial morphology

Afsaneh Fakhar | **Saeid Maghami** | **Elham Sameti** | **Monireh Shekari** | **Morteza Sadeghi**

Department of Chemical Engineering, Isfahan University of Technology, Isfahan, Iran

Correspondence
Afsaneh Fakhar and Morteza Sadeghi, Department of Chemical Engineering, Isfahan University of Technology, Isfahan 84156-83111, Iran.
Email: a.fakhar@iut.ac.ir (A. F.) and m-sadeghi@cc.iut.ac.ir (M. S.)

Abstract

A series of polyurethane/ZnO membranes was fabricated via thermal phase inversion of the solution of polymer/nanoparticle in *N*,*N*-dimethylformamide solvent. The polyurethane synthesis was done via two-step polymerization method using polytetramethylene glycol, isophorone diisocyanate, and 1,4-butanediol in the ratio of 1:3:2. Different concentrations of zinc oxide nanoparticles (5, 10, 15, and 20) were incorporated into the polyurethane matrix. FTIR, SEM, and X-Ray analysis were performed to characterize the membranes. FTIR and SEM results suggests an increment in the phase mixing of polyurethane with ZnO loading. Gas permeation performance through polyurethane-ZnO mixed matrix membranes with ZnO loading by as much as 20 wt% were elucidated for pure N_2, O_2, CH_4, and CO_2 and gases. Based on the results, all permeability values decreased as the loading of ZnO nanoparticles increased, whereas CO_2/N_2 and CO_2/CH_4 selectivities increased. Moreover, interfacial structure of the polyurethane/ZnO nanocomposites were characterized by molecular probing approach. The results revealed the presence of a rigidified polymer chain layer with 65 ± 6 Å thickness around the ZnO nanoparticles.

KEYWORDS

gas separation, interfacial morphology, membrane, polyurethane, ZnO nanocomposite

1 | INTRODUCTION

Polymeric gas separation membranes have attracted much attention in gas separation industry over the last few decades, due to their high gas separation efficiency, low capital investment, easy processing, and low energy consumption.[1–3] CO_2 capturing, hydrogen recovery from ammonia plant purge streams, helium separation from natural gas, separating air into its components to produce pure nitrogen are some examples of processes in which gas separation membranes are used.[4] The effect of different parameters like free volume content, glassy, and rubbery state of polymers, concentration of inorganic particles in membranes and operating condition on the gas separation performance through polymer membranes has been studied.[5–14]

The tradeoff between selectivity and permeability has limited the efficiency of pure polymeric membranes.[15,16] With the advancement of nanotechnology and synthesis of metal and metal oxide nanoparticles, tendency to use nanocomposites has been increased.[14,17] Incorporating inorganic nanoparticles into polymeric matrix will improve characteristics such as mechanical strength, thermal stability, hydrophilicity, antiviral, and antibacterial.[18–20] The polymer/nanoparticles based membranes named mixed matrix membranes (MMMs) are chemically stable, have high mechanical properties, and high separation efficiency. Various kinds of nanoparticles (SiO_2, TiO_2, ZrO_2, CeO, and ZnO) are commercially available to improve barrier properties of polymeric membranes.[18,21,22]

Controlling the free volume in glassy nanocomposite membranes can tailor the permeation properties. Higher free volume facilitates the gas molecule transport through the membrane. Gomes et al. expressed two probable transport mechanisms through fumed silica/PTMSP membranes based on the free volume: simultaneous increase in selectivity and permeability because of increased polymer free volume without non-selective flaws or increased permeability along with decreased selectivity because of increase in the free volume of polymer with non-selective channels.[23] As free volume decreases, gas molecules with larger size are more confined to permeate, which can result in permeability reduction and selectivity increment as expressed by Sadeghi et al.[24]

Since rubbery membranes mostly conduct gas separation via solubility mechanism, they are preferred for CO_2 capture compared to glassy ones.[25] Polyurethanes (PU)s are good category of rubbery membranes for CO_2 separation.[26,27] Polyurethanes are served in coatings, sealants, textiles, medical, and membrane industries. They provide excellent mechanical, toughness, and chemical properties. PU is a diblock copolymer, which consists of soft and hard domains. Because of hydrogen banding between hard domains, they act as crosslinks between the amorphous polyether (or polyester) soft segment domains. PUs express so attractive thermal and mechanical properties arising from the phase separation degree between their hard and soft segments and their chemical structure.[27,28] Polyurethane consists of phase-separated soft and hard segment domains. The phase separation degree affects mechanical and gas permeation behavior of polyurethane membranes. Higher phase separation is in favor of gas permeability.[25,29,30]

To raise the gas permeation properties of polyurethane membranes, various inorganic nanoparticles were employed in different researches. The influence of non-permeable nano-silica on PU gas separation was explored. O_2, N_2, CO_2, and CH_4 permeability values decrease as the particle loading increases, while CO_2/N_2, CO_2/CH_4, and O_2/N_2 selectivity values increased.[24] Increased gas selectivities and decreased permeabilities have been obtained by Titania incorporation in polyurethane.[31] Similar results were achieved by epoxy nanoparticles-based MMM.[14] Simultaneous enhanced selectivity and permeability through PU MMMs containing zeolites (4A, 3A, and ZSM-5) was obtained by Taheri Afarani et al.[32] Decrease in permeability along with increased selectivity by alumina nanoparticles/polyurethane MMMs was also reported.[33] The results revealed reduction in permeability and O_2/N_2, CO_2/N_2, and CO_2/CH_4 selectivity values with increasing alumina concentration. This is ascribed to interfacial polymer chain rigidification which confirmed by increment of glass transition temperature and increase in phase interferences via adhesion of nano-alumina according to FTIR spectra.[33] Porous silica (MCM-48, MCM-41, and SBA-16) modified by silane caused higher permeability with no substantial decrease in selectivity through polyurethane membranes.[34] Gas permeability coefficients through thermo-sensitive polyurethane (TSPU) membranes increased significantly as the loading of nano-TiO_2 increased based on Chen et al.'s study. Since the particles gives rise to make more tortuous route for gas diffusion in polymer, this observation was not explainable by conventional theory in which reduction in gas diffusion is expected. It was suggested that rigid chain of TSPU did not pack effectively around the particles, resulting in polymer chain dilution around the particles.[35] The influence of SiO_2 and TiO_2 nanoparticles on TSPU membranes were also investigated for WVP.[6,36] Xu et al. reported a reduction in WVP poly(urethane urea)s (PUU)s by a factor of five at 20% of organically modified layered silicate (OLS) loading.[37] The influence of nano-ZnO on gas separation performance of polyester PU has indicated that gas permeability increased by introduction of 0.5% ZnO, while it decreased for the 1% nanoparticle contained membrane.[38]

ZnO nanoparticles have specific features including easy to disperse, no surface water, high chemical stability, and low dielectric constant.[9,23,29,39] The influence of ZnO on oxygen separation through PMMA membranes was studied by Hess et al. No effect on O_2 permeability was observed, which could be attributed to large enough particle-free domains for gas transport without significant hindrance by the particles.[39] The presence of ZnO in polyurethane led to decrease in phase separation content between soft and hard domains. It might arise from the reaction between isocyanate groups in PU and hydroxyl groups on the surface of ZnO.[29] This causes more accessible NH groups in the hard segments reacting with soft domains, thereby higher phase mixing which increases the probability of the particle distribution in the hard

domains.[40,41] Increased phase mixing of polyurethane with ZnO content was also reported by Mishra et al.,[18] which resulted polymer chain rigidity around the particles.

In consequence, formation of a diluted or rigidified polymer chain layer around filler particles in nanocomposite materials can be resulted depend on the kind of the polymer matrix-filler particle interactions. In this regard, characterizing the role and nature of interfacial layer in polymer nanocomposites can give a profound knowledge about their resultant gas separation properties.

Since PU is an interesting diblock polymer with special characterization, the objective of this study is exploring the gas separation properties of PU-based MMMs containing ZnO nanoparticles. The influence of ZnO nanoparticle contents on permeability and selectivity through the MMMs was investigated. Higher selectivity through PU membranes in comparison with PUU encouraged us to use PU as the matrix by the purpose of increasing selectivity.[24] Finally, the presence of interfacial layer in the PU based MMMs was characterized by molecular probing approach using modified Maxwell model. The approach employs the gas permeation properties through the MMMs to characterize the thickness and effective permeation characteristic parameters of the interphase.

2 | EXPERIMENTAL

2.1 | Materials

1,4-butanediol (BDO), isophoronediisocyanate (IPDI) and *N*,*N*-dimethylformamide (DMF) were supplied by Merck. Liquid BDO was dried over 4°A molecular sieve prior to use. Polytetramethylene-glycol (PTMG, Mw = 2000 $gmol^{-1}$) was purchased from Arak petrochemical company (Arak, Iran) and dried at 85°C for 48 h under vacuum. ZnO nano powder (crystal size 50–70 nm and 45 m^2/g of special surface) was purchased from Nano Pars Spadana company (Isfahan, Iran). Gas permeation measurements were performed using 99.99% pure CO_2, N_2, and O_2 (Ardestan Gas Co., Tehran, Iran) and 99.5% pure CH_4 (TGS Co.).

2.2 | Polymer preparation

A two-step polymerization approach was used for polyurethane synthesis in bulk state. First, PTMG was reacted with IPDI at 85–90°C for 2 h under nitrogen to produce macrodiisocyanate prepolymer. Then, BDO as the chain extender was added to the reaction vessel at ambient temperature. The molar ratio of OH to NCO was kept 1 to obtain a linear polymer. The molar ratio of [PTMG]: [IPDI]: [BDO] = 1: 3: 2 was used. Scheme 1 shows the chemical structure of the synthesized polyurethane.

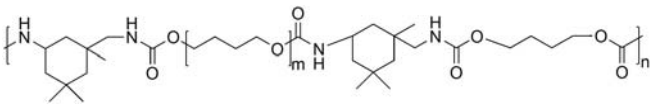

SCHEME 1 Chemical structure of the synthesized polymer

2.3 | Membrane preparation

For preparation of PU membrane, 10 g of polyurethane was dissolved in 90 g of DMF at 80°C under solvent refluxing condition for 2 h. Then, the solution was cast in Petri dish at ambient temperature. Finally, the membrane was prepared by solvent evaporation at 60°C for 24 h.

PU/ZnO membranes were fabricated by mixing of ZnO and PU in DMF solvent until a homogenous solution of 10 wt% polymer and nanoparticle/solvent was obtained. Nanoparticles were dispersed within the solution by vigorous stirring and sonication. The casted solution in a Petri dish was placed in an oven followed a procedure similar to PU membrane preparation.[42] Concentrations of 5, 10, 15, and 20 wt% ZnO were prepared using the same manner described above. The average thickness of the prepared membranes was measured as around 80 μm.

At higher loading of ZnO nanoparticles, viscosity of nanocomposite tends to decrease. Zheng and Kozisi showed that ZnO incorporation could lead to the decrease in elasticity, elastic modulus and size of polyurethane self-assemblies, while an increment in T_g of nanocomposite and dispersion of hard phase. Dispersion of hard segment prevents soft segments from entanglement, which leads to the reduction in viscosity.

2.4 | Characterization

To study the prepared membranes A BIO-RAD FTS-7 Fourier transform infrared spectrometer (FTIR) was served at room temperature and frequency range of 400–4000 cm^{-1}. Scanning electron microscopy (SEM) images were obtained by Philips XL30. All samples were coated with gold–palladium target. X-ray diffraction patterns were recorded by monitoring the diffraction angle 2θ (5–80°) on a Philips X'Pert (Netherlands) with Cu radiation under 40 mA current and 40 kV voltage. The presence of interfacial morphology in PU/ZnO nanocomposites was investigated by molecular probing approach where developed in our previous study.[43]

2.5 | Gas permeation tests

Constant pressure/variable volume method was used to determine the permeability of O_2, N_2, CH_4, and CO_2 at 25°C and 10 bars according to Equation (1).[24,44]

$$P = \frac{qL}{A(P_1 - P_2)}, \quad (1)$$

where P is permeability in Barrer (1 Barrer = 10^{-10} cm^3 [STP] cm/cm^2 s cm Hg), L is thickness of the membrane (cm), q is gas flow rate through the membrane (cm^3/s), A is membrane area (cm^2) and P_1 and P_2 are the absolute pressures of upstream and downstream side, respectively (cm Hg). The ratio of single gas permeabilities through the membranes was calculated as ideal selectivity:

$$\alpha_{A/B} = \frac{P_A}{P_B}, \quad (2)$$

The permeation of gases through dense polymers could be explained via well-known solution (S)-diffusion (D) mechanism where the permeability coefficient is defined according to the following equation.[45]

$$P = D \times S. \quad (3)$$

3 | RESULTS AND DISCUSSION

3.1 | FTIR analysis

The FTIR analysis has been done on the pure ZnO, polyurethane, and PU/ZnO nanocomposite. As shown in Figure 1, a broad peak appeared around 3100–3600 cm^{-1} in ZnO spectrum indicates the presence of alcohol group on the ZnO surface. The peak at the 500 cm^{-1} in ZnO spectrum appeared in all membranes' spectra which affirms the ZnO presence in all hybrid membranes.

The 3329 and 1110 cm^{-1} peaks corresponds to urethane NH group and symmetrical C—O—C groups, respectively. The peaks at 2935 and 2857 cm^{-1} could be attributed to C—H linkages.

A binary pick observed around 1698–1720 cm^{-1} is attributed to carbonyl groups in polyurethane. Binary pick was deconvoluted to two peaks at 1719 and 1700 cm^{-1} which attributes to free carbonyl group and bonded carbonyl group, respectively. Hydrogen bonding index (HBI) is defined by the ratio of absorbance intensity of bonded carbonyls to that of free carbonyls (Equation (1)) which quantifies the degree of phase separation. Higher HBI value favors the phase separation degree.

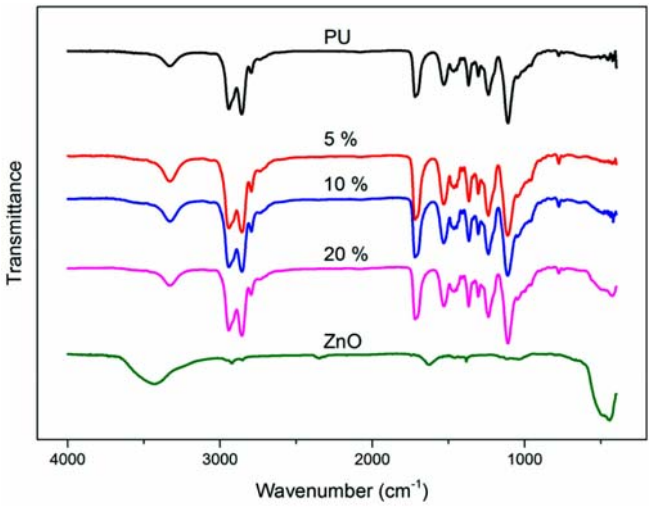

FIGURE 1 The FTIR spectra of zinc oxide, PU and PU-ZnO membranes

$$HBI = \frac{A_{C=O,\ bonded}}{A_{C=O,\ free}}, \quad (4)$$

The calculated HBI values after the peaks deconvolution using Origin software (Figure 2) is as follows:

Pure PU (5.82) > PU-2.5% (5.52) > PU-5% (5.42) > PU-10% (5.25) > PU-20% (4.71).

A little decrease in HBI values by increase the ZnO content in the membranes confirms decrease in phase separation. The hydroxyl groups on the ZnO surface can react with carbonyl groups in the hard segments. Therefore, less carbonyl groups are accessible for NH groups in the hard domain for hydrogen bonding. This increases the probable interaction between ether groups of soft domain and accessible NH groups of hard domains favoring phase mixing. Decrease in the phase segregation of PU membranes by incorporation of ZnO nanoparticles was achieved by others, too.[18,29]

3.2 | SEM analysis

The morphology of the prepared membranes and the nanoparticles distribution in the hybrid membranes was investigated by SEM analysis. Figures 3–5 show the SEM images of the cross section of prepared membranes with 5, 10, and 20 wt% of ZnO loading, respectively. The symmetric dense membranes have been made in all cases. Also, the uniform dispersion of particles in membranes has been evidenced.

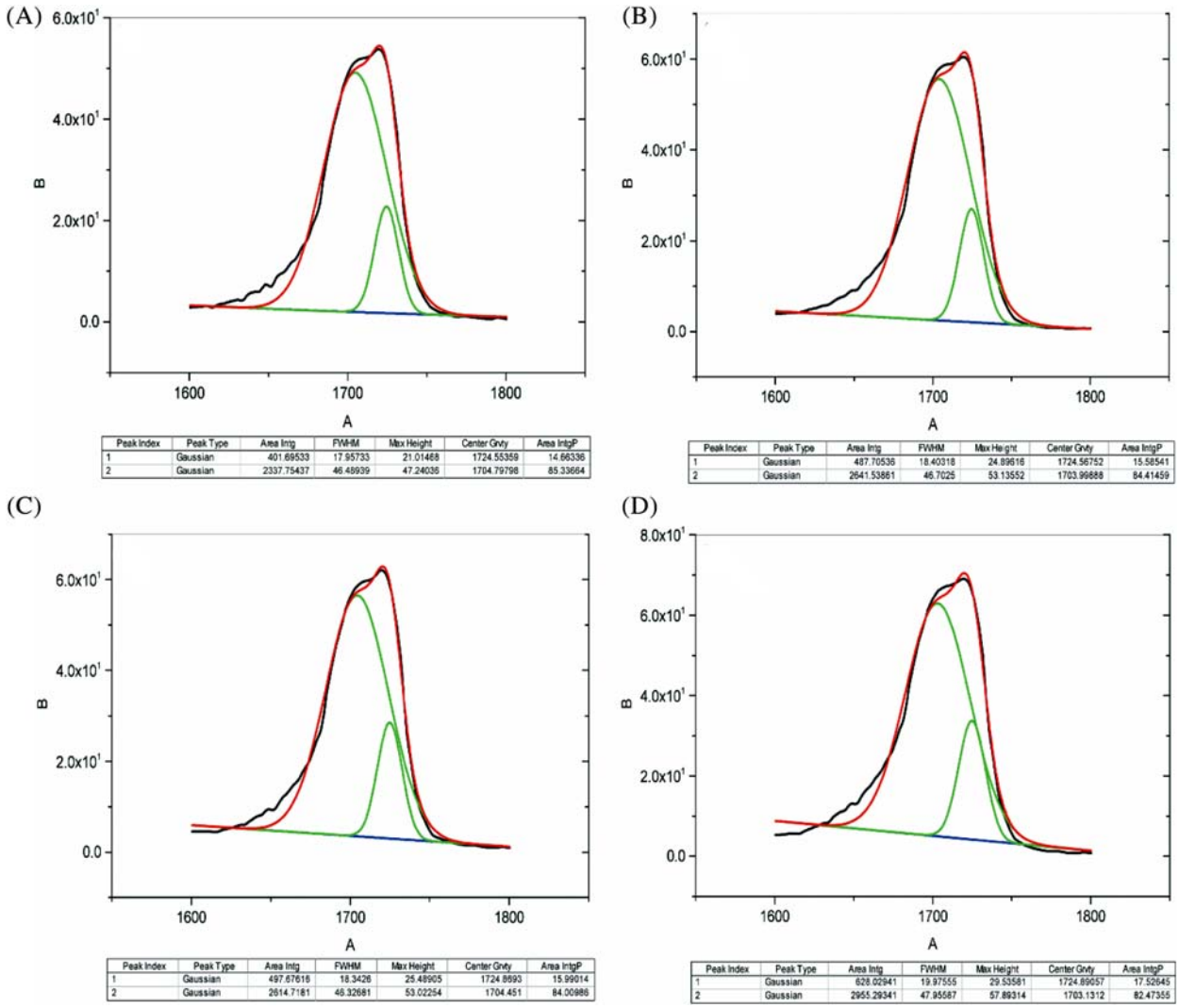

FIGURE 2 The deconvolution results of carbonyl groups for (A) pure PU, (B) PU-5%, (C) PU-10%, and (D) PU-20% membranes

From the SEM images, some cracks on the polymer surface attributed to the high voltage energy can be seen. The dispersed particles are appeared in hybrid membranes in two forms. Accumulated particles ranged from 100 to 300 nm while remaining particles ranged from 40 to 70 nm. These observations indicate the nano-scale distribution of ZnO particles in the presence of some particle accumulation in the hybrid membranes.

3.3 | XRD analysis

Wide-angle X-ray diffraction measurements were done to investigate the crystallinity of PU/ZnO membranes. Figure 6 indicates the X-ray diffraction patterns of the MMMs containing various ZnO concentration. Sharp diffraction peaks for ZnO and a broad peak for PU can be seen in All the patterns. The broad peak appeared around $2\theta = 20$ referred to amorphous morphology or scattering of the small size crystals distributed in amorphous regions.[46] As it has been depicted in Figure 6, the broad peak around $2\theta = 20$ was broadened by ZnO particles, which indicate the higher amorphous morphology of hybrid membranes. The intensity of the peaks related to ZnO particles increased at higher ZnO loading in the MMMs. The crystalline peaks of ZnO could correspond to the hexagonally structured ZnO. Absence of a new peak and no peak shift with respect to PU was obtained by the ZnO incorporation, which confirms that PU-based MMMs consist of two phase: polymer and nanoparticle. Scherrer formula estimates the average grain size (D) of ZnO:

$$D = k\left(\frac{\lambda}{\beta\cos\theta}\right), \tag{5}$$

where $\lambda = 0.154$ nm, $k = 0.89$ (Cu, Ka) and β is the full width at half maximum (FWHM) at a θ. Average grain size for the MMMs was obtained as 36 nm.

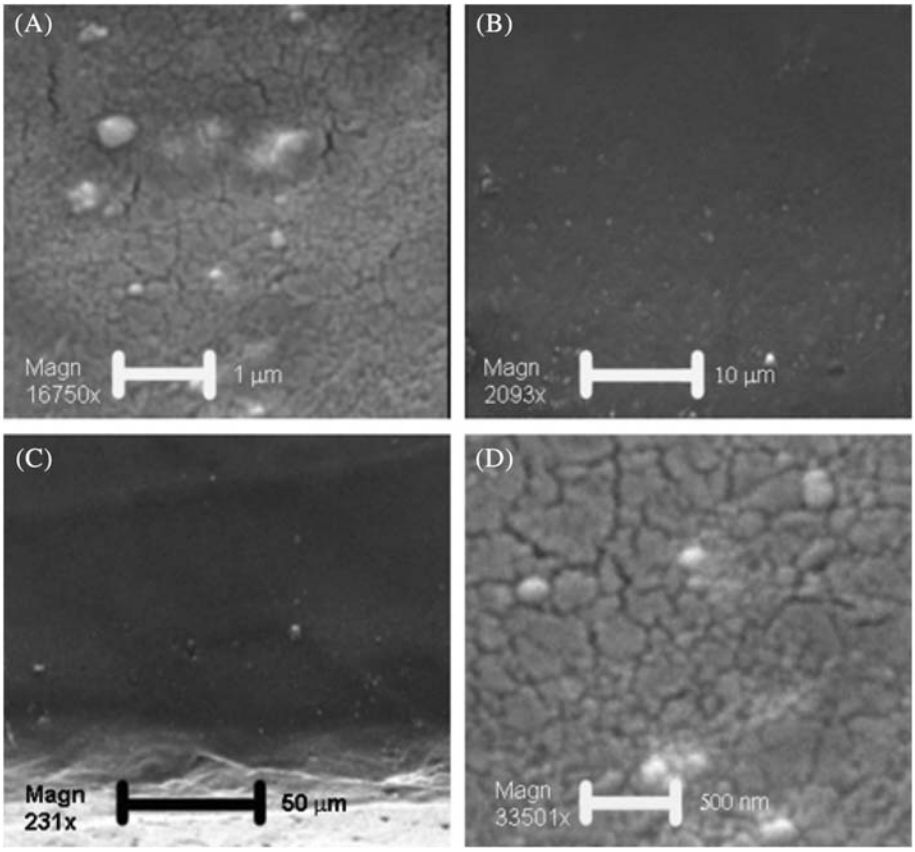

FIGURE 3 SEM picture of nanocomposite, 5 wt% ZnO, (A) 1 μm, (B) 10 μm, (C) 50 μm, and (D) 500 nm

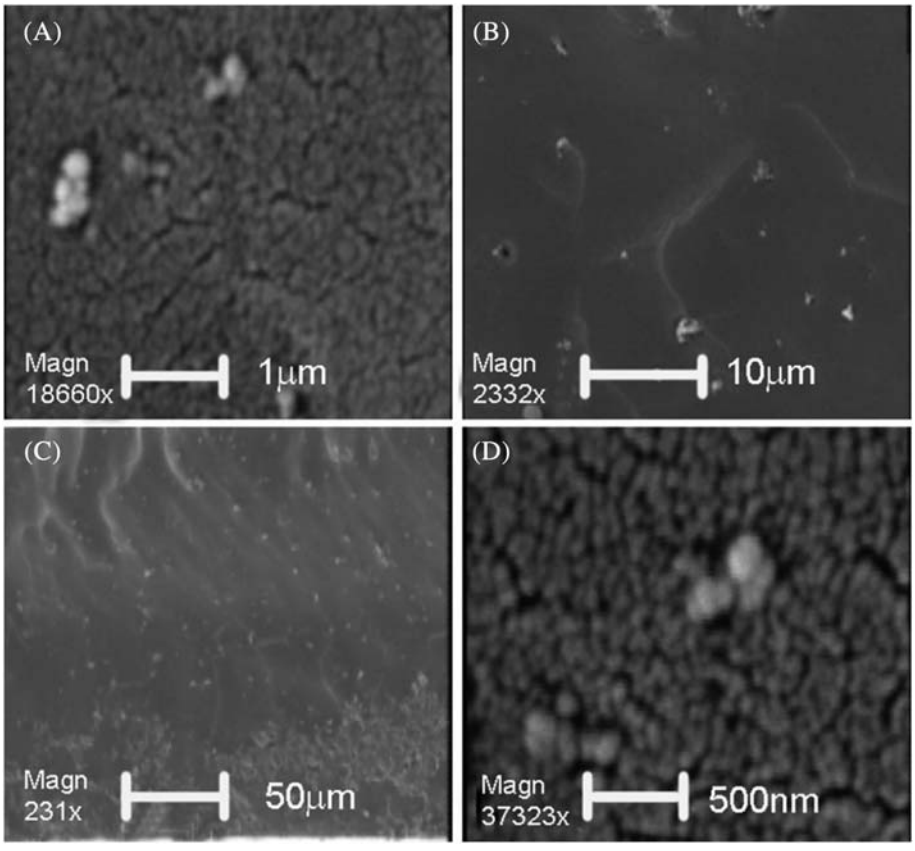

FIGURE 4 SEM picture of nanocomposite, 10 wt% ZnO, (A) 1 μm, (B) 10 μm, (C) 50 μm, and (D) 500 nm

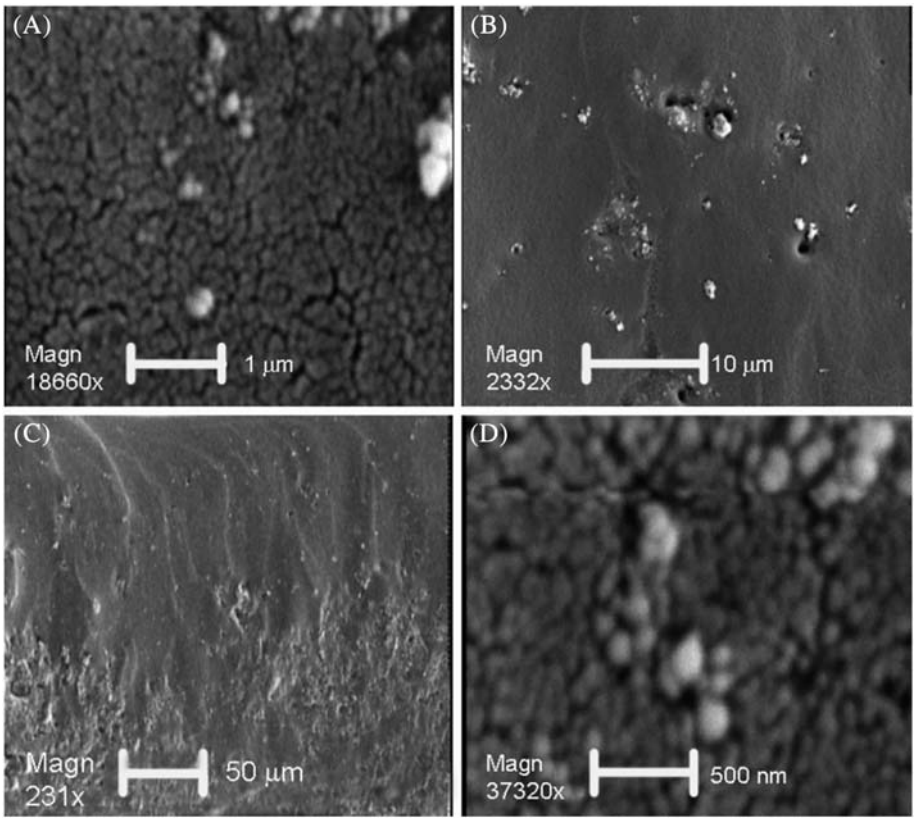

FIGURE 5 SEM picture of nanocomposite, 20 wt% ZnO, (A) 1 μm, (B) 10 μm, (C) 50 μm, and (D) 500 nm

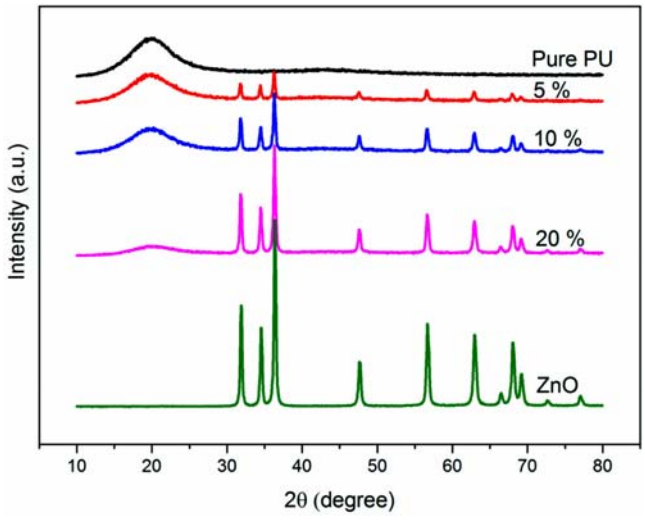

FIGURE 6 XRD patterns obtained for zinc oxide, PU and PU-ZnO hybrid membranes

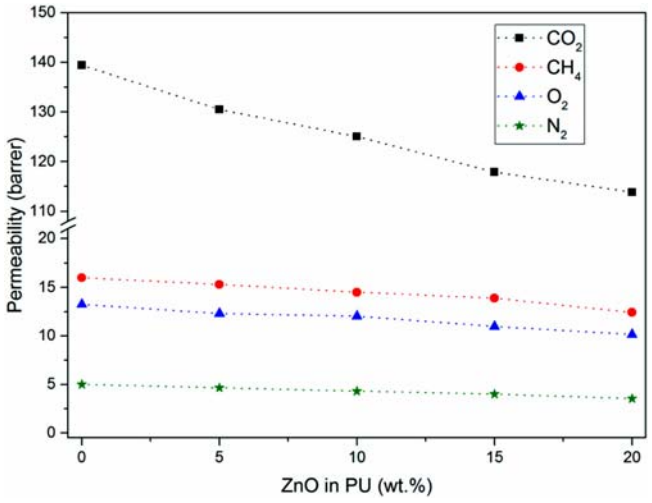

FIGURE 7 Permeability of N_2, O_2, CH_4, and CO_2 through PU and PU-ZnO membranes versus ZnO content

3.4 | Gas permeation

Figure 7 shows the effect of ZnO nanoparticles on N_2, CH_4, O_2, and CO_2 permeabilities through polyurethane/ZnO hybrid membranes. The permeability changes for all hybrid membranes according to the following order: P (CO_2)> > P (CH_4) > P (O_2) > P (N_2). Higher permeability of CO_2 is due to the relative high CO_2 solubility in the membranes when compared to CH_4, N_2, and O_2. In addition, CO_2 has a smaller molecular size compared to other gases. CO_2 is a polar gas that can interact with polar chain polymers.[47,48] Therefore, the permeability of CO_2 in hybrid membranes containing polar moieties in their structures is higher than other gases. In spite of larger diameter of CH_4 relative to the N_2 and O_2 molecules, it has higher

permeability (Figure 7). The CH_4 condensability is also higher than N_2 and O_2.

The diffusion coefficient of gases depends on gas molecular size and mobility of polymer chains, while gas sorption in polymer depends on gas affinity to the polymer, condensability of gas and active functional groups of the polymer. The latter may affect the gas transportation through polymer chains. Thus, the higher condensation temperature of CH_4 enhances its sorption in polymer leading to higher permeability in hybrid membranes as compared to N_2 and O_2. The results confirm that the solubility is the main mechanism in gas permeation through the studied hybrid membranes.

It is accepted in PU membranes the soft domains are permeable to molecules, while the hard domains are barrier. However, hard segment due to having ability to act as physical crosslinks and alter the soft domain dynamics can affect the overall gas permeation properties of PU.[49]

In polyurethane-ZnO nanocomposite membranes, there are soft and hard domains available for ZnO distribution. It appears ZnO nanoparticles distribute preferably in the hard segments of PU, based on entropic viewpoint.[46,50] Based on Figure 7 the gas permeability in all membranes decreased as the ZnO content increased. Therefore, it seems that the nanoparticles are mostly distributed in soft phase, which leads to a decrease in gas permeability as because of the impermeability of ZnO particles. The presence of non-permeable ZnO particles decreases the free volume of soft domains and hence gas molecule pass ways. In our previous works, we found that the metal oxide particles, like SiO_2 is mostly like to distribute in the soft phase which is consistent to obtained results here.[28]

Figure 7 compares the gas permeability in pure membrane and the MMMs. The permeability of CO_2, CH_4, O_2, and N_2 in the pure membrane decrease from 139.42, 16, 13.25 and 5 barrer to 113.83, 12.42, 10.15, and 3.53 barrer in the polyurethane-ZnO (20 wt%) hybrid membranes, respectively. The percentage of permeability reduction of the hybrid membranes with respect to neat PU could be expressed in the following order:

$$CO_2\,(18.3\%) < CH_4\,(22.3\%) < O_2\,(23.4\%) < N_2\,(29.4\%). \quad (6)$$

By reduction in free volume of polymer, gas molecules with larger size are more confined to pass through the polymer which results in higher decrease in their permeability compared to smaller size ones.[49] Consequently, higher decrease in N_2 permeability compared to CO_2 and O_2 is arising from its larger size and the presence of non-permeable ZnO. Contrary to the N_2, less decline in CH_4 permeability with larger size respect to N_2 and O_2 could be corresponded to higher CH_4 condensability in the PU and its hybrid membrane.

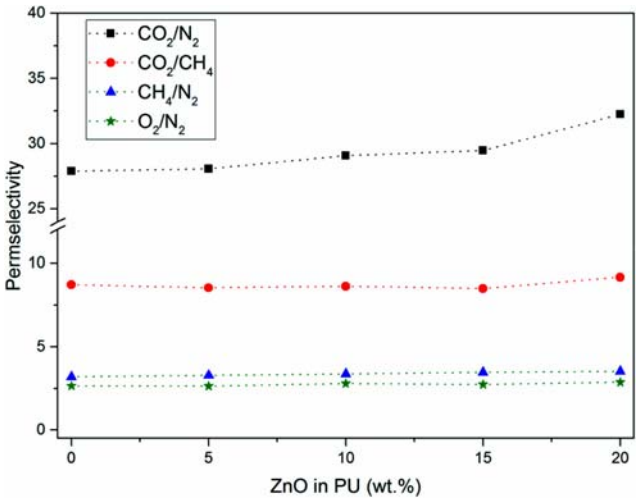

FIGURE 8 Permselectivity of CO_2/CH_4, CO_2/N_2, O_2/N_2, and CH_4/N_2 gases through PU and PU-ZnO membranes versus ZnO content

ZnO nanoparticles having non-organic nature can create some suitable spaces for dissolution of condensable gases in the organic polymer and non-organic particles interface. Thus, by increasing the ZnO content, dissolution of condensable CH_4 gas would increase, and unlike its larger kinetic diameter than O_2 and N_2, reduction in CH_4 permeability is slower.

FTIR spectra of ZnO samples showed the presence of OH groups in ZnO nanoparticles, which give suitable sites for polar gas dissolution. The less permeability reduction of carbon dioxide in comparison to others is because of both its smaller kinetic diameter and its higher dissolution in membrane. This could be attributed to the polar OH groups formed by ZnO nanoparticles.

Figure 8 shows the graph of selectivity for different pure gases through PU membranes. As shown, selectivity of O_2/N_2, CO_2/CH_4, and CH_4/N_2 gas pairs increased slowly by enhancing ZnO content up to 20 wt%. While, CO_2/N_2 selectivity of increased sharply at 20 wt% ZnO loading. Indeed, CO_2/N_2, CO_2/CH_4, O_2/N_2, and CH_4/N_2 selectivity values increased from 27.9, 8.7, 2.7, and 3.2 to 32.2, 9.2, 2.9, and 3.5 which show 17.9%, 5.7%, 7.4%, and 9.4% increment, respectively. The higher increment in CO_2/N_2 selectivity compared to other pair gases is related to the differences between molecular size and condensability of these pair gases.

Regarding the high energy cost, membrane technology is an economic option for different applications. CO_2

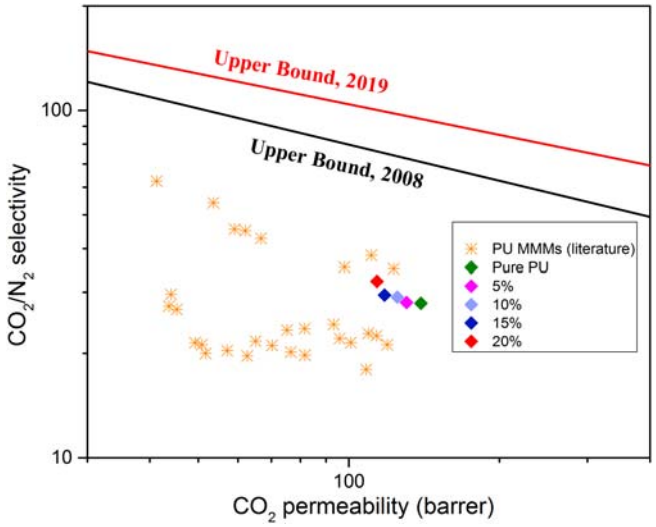

FIGURE 9 Upper bound correlation for CO_2/N_2 separation

separation from other gases in industrial processes is an important application and CO_2/N_2 separation for flue gas application is more considerable.[51] It was found that reduction in selectivity is generally accompanied with increment in permeability. The mentioned trade-off was related to an upper bound relationship when separation factor was plotted versus permeability in a log–log scale for polymer membranes.[1,4] The upper bound relationship is expressed by:

$$P_i = k\alpha_{ij}, \tag{7}$$

where P_i is the permeability of the more permeable gas, α_{ij} is the selectivity (P_i/P_j) and k is the slope of the log–log limit.

The Robeson's diagram of our experiment in Figure 9 shows economic benefits with increasing percent of ZnO nanocomposite.

3.5 | Interfacial characterization

Existence of an interfacial layer around filler particles in polymer/particle composites has been confirmed in many studies. This layer forms as a result of the attractive or repulsive interactions between polymer chains and filler particles. Since separation properties of MMMs are impressed by presence of an interfacial layer in their structure, characterization of the interphase helps to understand the structure–property relationships of the composites. In our previous work we developed a new approach for this purpose.[43] In our method, gas molecules are employed as probes to determine the changes in dynamics of polymer chains around the particles. By measuring gas transport properties of the composites, their macroscopic permeation properties can be described in terms of their microscopic properties. In this method effective permeability of the MMM is expressed by modified Maxwell model as follows:

$$P_{eff} = P_c\left(\frac{1+2\Phi_{ps}\lambda_{eff}}{1-\Phi_{ps}\lambda_{eff}}\right), \tag{8}$$

$$\lambda_{eff} = \frac{P_{ps}-P_c}{P_{ps}+2P_c}, -0.5 \le \lambda_{eff} \le 1, \tag{9}$$

$$P_{ps} = P_I\left(\frac{1+2\Phi_2\lambda_{ps}}{1-\Phi_2\lambda_{ps}}\right), \tag{10}$$

$$\lambda_{ps} = \frac{P_{dB}-P_I}{P_{dB}+2P_I}, -0.5 \le \lambda_{ps} \le 1, \tag{11}$$

$$\Phi_2 = \frac{\Phi_d}{\Phi_{ps}=\Phi_d+\Phi_I} = \frac{{r_d}^3}{(r_d+l_I)^3}, 0 \le l_I \le l_{max}, \tag{12}$$

$$P_I = \beta \times P_c, 0 \le \beta \le \beta_{max}, \tag{13}$$

$$P_{dB} = \gamma \times P_d, 0 \le \gamma \le 1, \tag{14}$$

where, P_c and P_{ps} are the respective permeability of the matrix and surrounded particles by interphase. P_I and P_{dB} represent the permeabilities of the interface layer and the particles impressed by pore blockage, respectively. Besides, Φ_{ps} and Φ_I indicate the volume fraction of the surrounded particles by interphase and interphase in the composite, respectively, and Φ_2 is the volume fraction of the particles in the surrounded particles by interphase. γ is the permeability reduction factor of the impressed particles by blockage, β is the permeability adjustment factor of the interphase, l_I is the thickness of interfacial layer and r_d is the mean radius of filler particles. It is notable that since ZnO nanoparticles are impermeable, $P_d = P_{dB} = 0$ and β_{max} which represents the maximum permeability correction factor of the interphase is correspond to 1 due to good affinity of the particles with PU. In the case of polymer chain dilution β_{max} is determined by parallel model as described in our previous work.[43] Moreover, l_{max} is a large enough interphase thickness to achieve the global minimum in the plot of percentage of average absolute relative error (*%AARE*) versus l_I (see Figure 10(B)).

In the following, permeability of the MMM for $0 \le l_I \le l_{max}$ and $0 \le \beta \le 1$ is calculated using Equations (8)–(14) and computing absolute relative error (*ARE*) correspond to each values of β and l_I for gas *i*:

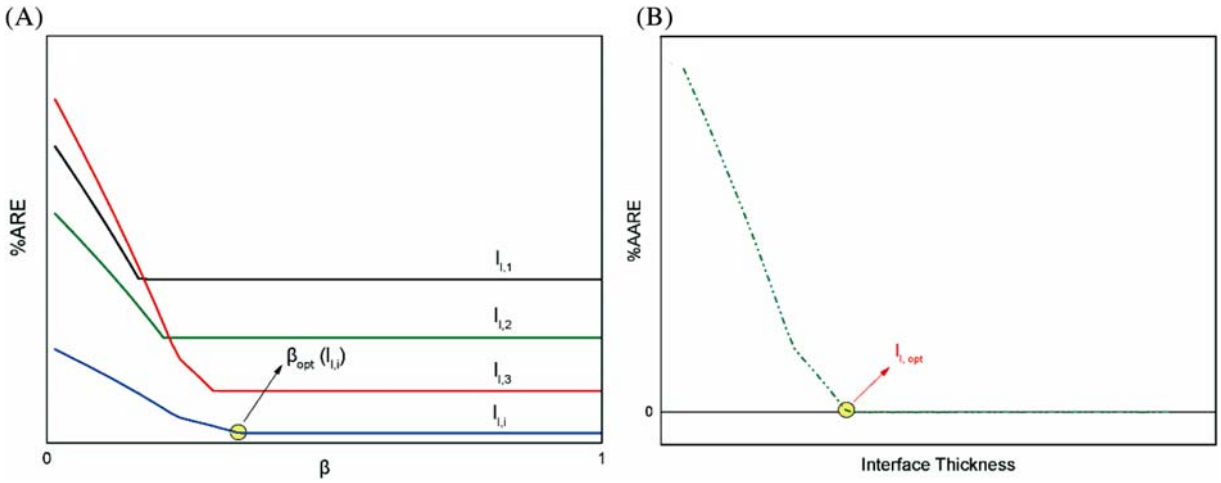

FIGURE 10 (A) Plot of *%ARE* versus β for different values of l_I, and (B) plot of *%AARE* versus l

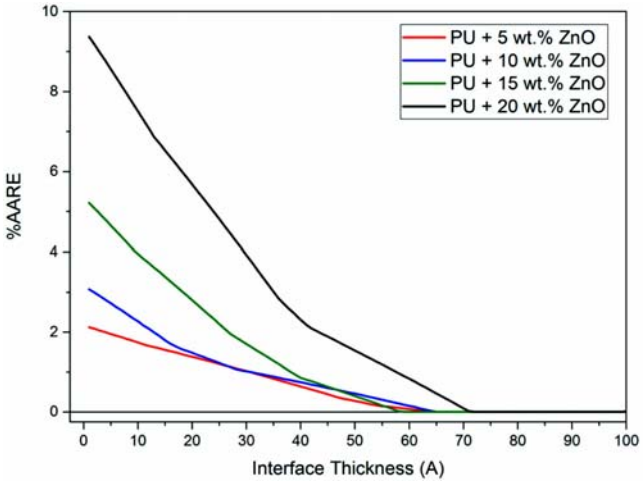

FIGURE 11 Plots of *%AARE* versus l_I using modified Maxwell model in PU/ZnO MMMs

$$ARE(i,\beta,l_I)=\left|\frac{P_{eff,i}-P_{exp,i}}{P_{exp,i}}\right|. \tag{15}$$

Next, as illustrated in Figure 10(A), for every gas, optimal value of β, β_{opt}, correspond to each of the values l_I is obtained according to the global minimum of *ARE* (i, β, l_I).

Finally, *%AARE*(l_I) is calculated as:

$$\%AARE(l_I)=\frac{100}{N}\sum_{i=1}^{N}ARE\left(i,\beta_{opt},l_I\right), \tag{16}$$

where N is the number of the gasses.

As shown in Figure 10(B), the overall minimum seen in the plot of *%AARE* versus l_I relates to the optimum interphase thickness ($l_{I.\ opt}$). Now, after determining $l_{I.\ opt}$, the optimal values of β_i for each gas is obtained.

TABLE 1 The optimal values of β in PU/ZnO MMMs using the proposed method and modified Maxwell model

	β_{opt}			
Φ_d (wt%)	CO_2	O_2	N_2	CH_4
5	0.18	0.29	0.01	0.84
10	0.58	0.77	0.00	0.74
15	0.55	0.33	0.01	0.85
20	0.82	0.43	0.00	0.50

The variations of *%AARE* versus l obtained from employing the proposed method for experimental permeation data of the PU/ZnO MMMs presented in Figure 11. As revealed, the mean thickness of the interphase in PU/ZnO MMMs are 66, 65, 59, and 71 Å for the respective nanocomposites containing 5, 10, 15, and 20 wt% ZnO. Table 1 represents the optimal values of β for under studied gases. As indicated, the interfacial polymer chain rigidification has the highest influence on N_2 permeation. This can be attributed to the molecular size and the lower condensability nature of N_2 compared to other gases.

According to our previous modeling approach after determining an interphase thickness, effective permeability of the nanocomposites can be predictable by only adjusting λ_{eff} in the range of −0.5 to 1 in modified Maxwell model.[52] As indicated in Figure 12, the accuracy of predictions of modified Maxwell model using $l_{I.\ opt}$ correspond to the composite containing 20 wt% ZnO is more than 98%. In consequence, our modeling approach is capable to predict gas transport properties through the

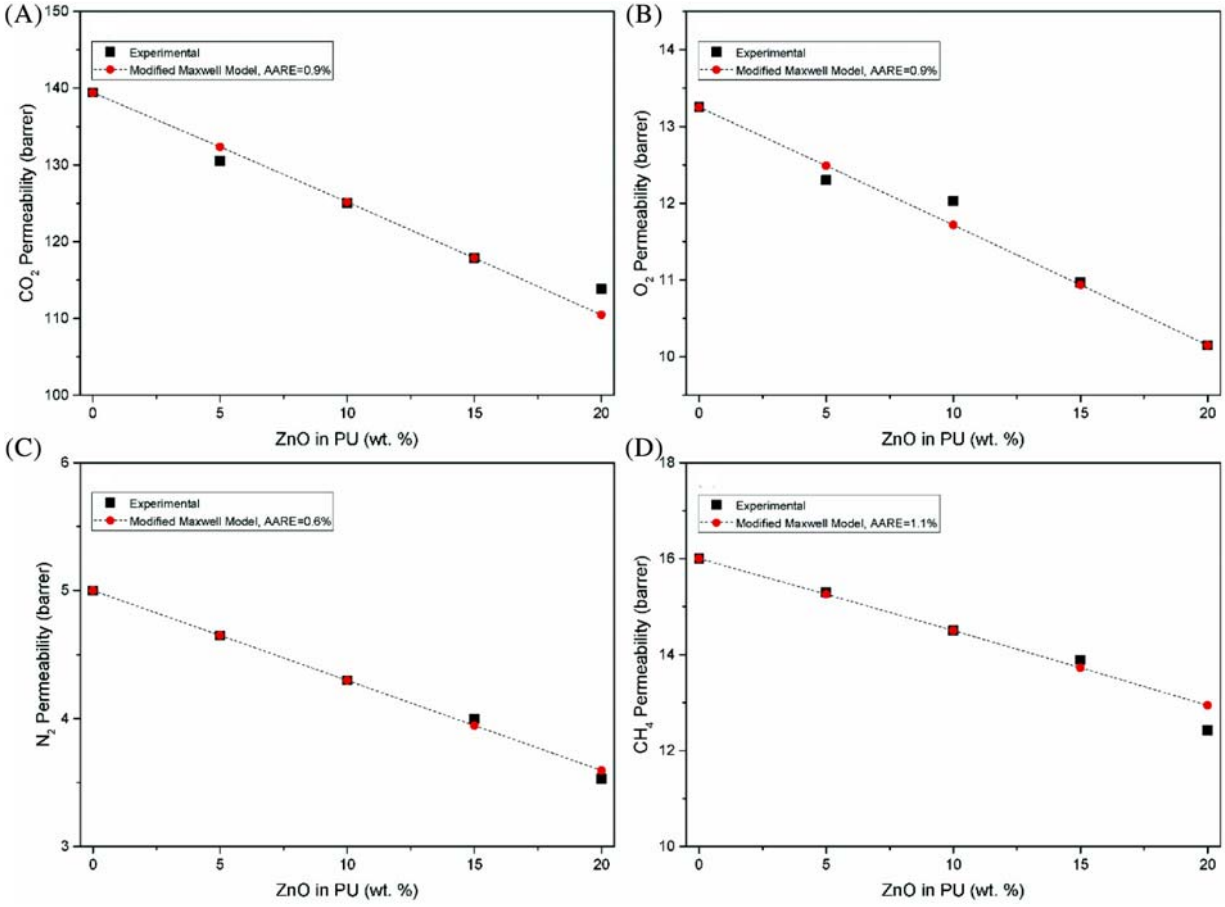

FIGURE 12 Comparison of the experimental data by the predictions of modified Maxwell models

MMMs at particle loadings lower than 20 wt% by only using experimental data correspond to it. The modeling method resulted the optimal values of 0.62, 0.43, 0.08 for CO_2, O_2, N_2, and CH_4, respectively and 0.76 for β.

4 | CONCLUSIONS

The MMMs containing ZnO nanoparticles with different contents were fabricated for the purpose of gas separation. The membranes were characterized by SEM, FTIR and X-Ray analyses. Moreover, since the smallest variations in polymer chain packing can be realized by Angstrom-size gaseous penetrants, the interfacial morphology in the PU/ZnO MMMs was characterized by molecular probing approach using modified Maxwell model. SEM micrographs indicated good dispersion of ZnO nanoparticles in PU. Gas separation properties of polyurethane- ZnO nanocomposite membrane with ZnO content up to 20 wt% were studied for pure N_2, O_2, CH_4, and CO_2 gases. The results indicated a decrease in permeability of all gases and increase in CO_2/N_2 and CO_2/CH_4 gas selectivity upon increasing the ZnO content. Comparing the obtained gas separation properties of the fabricated MMMs with the Upper bound indicates their proper capability commercialization. Higher ZnO loaded membranes were located closer to the Upper bound indicating their better gas separation performance. Applying the molecular probing method resulted the presence of a rigidified polymer chain layer around nanoparticles of ZnO with 65 ± 6 Å thickness. Besides, permeation properties of the nanocomposites were estimated by modified Maxwell model and determining 71 Å thickness for the interphase correspond to the composite containing 20 wt % ZnO. The obtained results revealed that not only effective permeability of the nanocomposites predicted with good accuracy (higher than 98%), but also minimize the number of experiments to predict properly permeation properties of the composites containing particle loadings lower than 20 wt%.

ORCID

Afsaneh Fakhar https://orcid.org/0000-0003-1867-8197
Morteza Sadeghi https://orcid.org/0000-0002-0075-1520

REFERENCES

[1] K. Madhavan, B. S. R. Reddy, *J. Membr. Sci.* **2009**, *342*, 291.
[2] B. Haider, M. R. Dilshad, M. A. u. Rehman, M. S. Akram, M. Kaspereit, *J. Nat. Gas Sci. Eng.* **2020**, *81*, 103406.
[3] S. Mosleh, M. Mozdianfard, M. Hemmati, G. Khanbabaei, *Polym. Compos.* **2017**, *38*, 1363.
[4] L.-S. Teo, C.-Y. Chen, J.-F. Kuo, *J. Membr. Sci.* **1998**, *141*, 91.
[5] M. Ulbricht, *Polymer* **2006**, *47*, 2217.
[6] H. Zhou, Y. Chen, H. Fan, H. Shi, Z. Luo, B. Shi, *J. Appl. Polym. Sci.* **2008**, *109*, 3002.
[7] H. Cong, M. Radosz, B. F. Towler, Y. Shen, *Sep. Purif. Technol.* **2007**, *55*, 281.
[8] L. M. Robeson, *Ind. Eng. Chem. Res.* **2010**, *49*, 11859.
[9] S. Awad, H. Chen, G. Chen, X. Gu, J. L. Lee, E. E. Abdel-Hady, Y. C. Jean, *Macromolecules* **2011**, *44*, 29.
[10] V. Mozaffari, M. Sadeghi, A. Fakhar, G. Khanbabaei, A. F. Ismail, *Sep. Purif. Technol.* **2017**, *185*, 202.
[11] A. Pournaghshband Isfahani, B. Ghalei, K. Wakimoto, R. Bagheri, E. Sivaniah, M. Sadeghi, *J. Mater. Chem. A* **2016**, *4*, 17431.
[12] M. Shahrooz, M. Sadeghi, R. Bagheri, M. Laghaei, *Macromolecules* **2016**, *49*, 4220.
[13] M. Laghaei, M. Sadeghi, B. Ghalei, M. Shahrooz, *J. Membr. Sci.* **2016**, *513*, 20.
[14] A. Pournaghshband Isfahani, M. Sadeghi, A. H. Saeedi Dehaghani, M. A. Aravand, *J. Ind. Eng. Chem.* **2016**, *44*, 67.
[15] A. D. Kiadehi, M. Jahanshahi, A. Rahimpour, H. Amir, S. Dehaghani, A. A. Ghoreyshi, *Chem. Eng. Process.* **2015**, *90*, 41.
[16] J. Hou, X. Li, R. Guo, Y. Qin, J. Zhang, *Polym. Compos.* **2018**, *39*, 4486.
[17] A. Soleimany, S. S. Hosseini, F. Gallucci, *Chem. Eng. Process.* **2017**, *122*, 296.
[18] A. K. Mishra, R. S. Mishra, R. Narayan, K. V. S. N. Raju, *Prog. Org. Coat.* **2010**, *67*, 405.
[19] I. Tirouni, M. Sadeghi, M. Pakizeh, *Sep. Purif. Technol.* **2015**, *141*, 394.
[20] M. Sadeghi, M. Mehdi Talakesh, B. Ghalei, M. Shafiei, Preparation, characterization and gas permeation properties of a polycaprolactone based polyurethane-silica nanocomposite membrane, *J. Membr. Sci.* **2013**, *427*, 21.
[21] M. Khoshkam, M. Sadeghi, M. P. Chenar, M. Naghsh, M. J. N. Fard, M. Shafiei, *RSC Adv.* **2016**, *6*, 35751.
[22] C. Hamciuc, E. Hamciuc, D. Rusu, M. Asandulesa, A. Wolinska-Grabczyk, *Polym. Compos.* **2018**, *39*, 1544.
[23] D. Gomes, S. P. Nunes, K.-V. Peinemann, *J. Membr. Sci.* **2005**, *246*, 13.
[24] M. Sadeghi, M. A. Semsarzadeh, M. Barikani, M. Pourafshari Chenar, *J. Membr. Sci.* **2011**, *376*, 188.
[25] A. Fakhar, M. Sadeghi, M. Dinari, R. Lammertink, *J. Membr. Sci.* **2019**, *574*, 136.
[26] S. M. Morozova, A. S. Shaplov, E. I. Lozinskaya, D. Mecerreyes, H. Sardon, S. Zulfiqar, F. Suárez-García, Y. S. Vygodskii, *Macromolecules* **2017**, *50*, 2814.
[27] M. Sadeghi, M. A. Semsarzadeh, M. Barikani, B. Ghalei, *J. Membr. Sci.* **2010**, *354*, 40.
[28] H. B. Park, C. K. Kim, Y. M. Lee, *J. Membr. Sci.* **2002**, *204*, 257.
[29] J. Zheng, R. Ozisik, R. W. Siegel, *Polymer* **2005**, *46*, 10873.
[30] A. Fakhar, M. Sadeghi, M. Dinari, M. Zarabadipoor, R. Lammertink, *Eur. Polym. J.* **2019**, *122*, 109346.
[31] M. Sadeghi, H. T. Afarani, Z. Tarashi, *Korean J. Chem. Eng.* **2015**, *32*, 97.
[32] H. T. Afarani, M. Sadeghi, A. Moheb, *Adv. Polym. Tech.* **2018**, *37*, 339.
[33] E. Ameri, M. Sadeghi, N. Zarei, A. Pournaghshband, *J. Membr. Sci.* **2015**, *479*, 11.
[34] B. Ghalei, A. Pournaghshband Isfahani, M. Sadeghi, E. Vakili, A. Jalili, *Polym. Advan. Technol.* **2018**, *29*, 874.
[35] Y. Chen, R. Wang, J. Zhou, H. Fan, B. Shi, *Polymer* **2011**, *52*, 1856.
[36] H. Zhou, Y. Chen, H. Fan, H. Shi, Z. Luo, B. Shi, *J. Membr. Sci.* **2008**, *318*, 71.
[37] R. Xu, E. Manias, A. J. Snyder, J. Runt, *J. Biomed. Mater. Res. A* **2003**, *64A*, 114.
[38] B. Soltani, M. Asghari, *Membranes* **2017**, *7*, 43.
[39] S. Hess, M. M. Demir, V. Yakutkin, S. Baluschev, G. Wegner, *Macromol. Rapid Commun.* **2009**, *30*, 394.
[40] A. Fakhar, M. Dinari, R. Lammertink, M. Sadeghi, *Sep. Purif. Technol.* **2020**, *241*, 116734.
[41] M. Sadeghi, A. Arabi Shamsabadi, A. Ronasi, A. Pournaghshband Isfahani, M. Dinari, M. Soroush, *Chem. Eng. Sci.* **2018**, *192*, 688.
[42] C. V. Rijn, *Nano and Micro Engineered Membrane Technology*, Elsevier Science, Amsterdam, The Netherlands **2004**.
[43] S. Maghami, M. Shahrooz, A. Mehrabani-Zeinabad, B. Zornoza, M. Sadeghi, *Polymer* **2020**, *205*, 122792.
[44] A. Khosravi, M. Sadeghi, *J. Membr. Sci.* **2013**, *434*, 171.
[45] P. Pandey, R. S. Chauhan, *Prog. Polym. Sci.* **2001**, *26*, 853.
[46] F. W. Billmeyer, *Textbook of Polymer Science*, Wiley, New York, NY **2000**.
[47] C. J. Orme, M. K. Harrup, T. A. Luther, R. P. Lash, K. S. Houston, D. H. Weinkauf, F. F. Stewart, *J. Membr. Sci.* **2001**, *186*, 249.
[48] L. Abdellah, B. Boutevin, F. Guida-Pietrasanta, M. Smaihi, *J. Membr. Sci.* **2003**, *217*, 295.
[49] M. Sadeghi, M. A. Semsarzadeh, M. Barikani, H. Moadel, *Iran. Polym. J* **2007**, *16*, 819.
[50] L. Sperling, *Introduction to Physical Polymer Science*, Wiley, New York, NY **2006**.
[51] L. M. Robeson, *J. Membr. Sci.* **2008**, *320*, 390.
[52] S. Maghami, M. Sadeghi, A. Mehrabani-Zeinabad, M. Zarabadi, B. Ghalei, *Ind. Eng. Chem. Res.* **2019**, *58*, 11022.

How to cite this article: Fakhar A, Maghami S, Sameti E, Shekari M, Sadeghi M. Gas separation through polyurethane–ZnO mixed matrix membranes and mathematical modeling of the interfacial morphology. *SPE Polymers*. 2020;1: 113–124. https://doi.org/10.1002/pls2.10023